Letter

Quantum vacuum effects in nonrelativistic quantum field theory

Matthew Edmonds,[1,2,*] Antonino Flachi,[3,2,†] and Marco Pasini[4,2,‡]

[1]*ARC Centre of Excellence in Future Low-Energy Electronics Technologies, School of Mathematics and Physics, University of Queensland, St Lucia, QLD 4072, Australia*

[2]*Research and Education Center for Natural Sciences, Keio University, 4-1-1 Hiyoshi, Yokohama, Kanagawa 223-8521, Japan*

[3]*Department of Physics, Keio University, 4-1-1 Hiyoshi, Yokohama, Kanagawa 223-8521, Japan*

[4]*Department of Mathematics, Computer Science, and Physics, University of Udine, Via delle Scienze 206 I-33100 Udine, Italy and INFN, via Valerio 2 - 34127 Trieste, Italia*

(Received 25 August 2023; accepted 11 October 2023; published 11 December 2023)

Nonlinearities in the dispersion relations associated with different interactions designs, boundary conditions, and the existence of a physical cutoff scale can alter the quantum vacuum energy of a nonrelativistic system nontrivially. As a material realization of this, we consider a one-dimensional-periodic rotating, interacting nonrelativistic setup. The quantum vacuum energy of such a system is expected to comprise two contributions: a fluctuation-induced quantum contribution and a repulsive *centrifugal-like* term. We analyze the problem in detail within a complex Schödinger quantum field theory with a quartic interaction potential and perform the calculations nonperturbatively in the interaction strength by exploiting the nonlinear structure of the associated nonlinear Schrödinger equation. Calculations are done both in zeta-regularization as well as by introducing a cutoff scale. We find a generic, regularization-independent behavior, where the competition between the interaction and rotation can be balanced at some critical ring size, where the quantum vacuum energy has a maximum and the force changes sign. The inclusion of a cutoff smoothes out the vacuum energy at small distance but leaves unaltered the long-distance behavior. We discuss how this behavior can be tested with ultracold atoms.

DOI: 10.1103/PhysRevD.108.L121702

Introduction. In quantum field theory, the canonical quantization scheme does not fix the order of noncommuting operators in the Hamiltonian, leaving a residual divergent *zero-point energy* contribution to the energy density (in natural units),

$$\mathscr{E} = \frac{1}{2}\sum_n \omega_n, \tag{1}$$

with ω_n representing the frequencies of the quantum fluctuations. Wick's normal ordering is then used to enforce a specific order of operators' products, resulting in the subtraction of this infinite shift from the vacuum expectation value (vev) of the Hamiltonian that will then vanish. This has the consequence that the quantum vacuum, *so defined*, does not carry energy, linear, or angular momentum. Such a procedure is usually justified by saying that a constant shift in the energy cannot be measured, although this view is not entirely tenable as any finite energy is, in principle, measurable due to its gravitational effect. In relativistic quantum field theory, a better justification follows from the fact that the expectation value of the Hamiltonian in the *noninteracting* vacuum (i.e., in the absence of external fields or interactions) must vanish for the Hamiltonian, *a* generator of the Poincaré group, to satisfy the correct commutation rules. Then, the usual notion of a noninteracting vacuum as a state devoid of energy follows, justifying the use of normal ordering [1,2].

Even without calling gravity into question [3], a variety of quantum vacuum phenomena, most notably the Casimir effect [4], clearly demonstrates some level of inadequacy of the above definition of an *empty* physical vacuum *tout court*. In the original version of the Casimir effect, for example, this was evident owing to the imposition of boundary conditions on the quantum fluctuations of the electromagnetic field in the presence of perfectly conducting, parallel plates, resulting in an attractive force between the plates. More general (and realistic) situations are not different, as boundary conditions result from quantum fields existing in interaction with other fields, and modify the spectrum of the quantum fluctuations, thus changing the zero-point energy.

*m.edmonds@uq.edu.au
†flachi@phys-h.keio.ac.jp
‡marco.pasini@uniud.it

These arguments converge into Casimir's definition of the energy of the quantum vacuum $E_{\rm vac}$ as the difference between the zero-point energies in the presence, $E[\partial B]$, and in the absence, $E[\emptyset]$, of boundaries, $E_{\rm vac} = E[\partial B] - E[\emptyset]$. Such a definition is compatible with the vanishing of the vev of the Hamiltonian in the noninteracting vacuum (i.e., no boundaries) and gives a calculable recipe of the quantum vacuum energy in response to changes in external conditions [2,5,6]. This view on the complexity of the vacuum has been vindicated during the past quarter of a century by many successful experiments starting with [7–9] (see also Ref. [10] for a recent additional list of examples of applications to nanophotonics, nanomechanics, and chemistry as well as Ref. [11] for a recent proposal connecting the quantum vacuum and interferometry.).

A less explored question concerns the quantum vacuum energy in nonrelativistic systems (see, for some discussions, Refs. [12–17]. The answer might seem simple, since in a nonrelativistic context there is no issue associated with antiparticles or the ordering of the operators, suggesting that the zero-point energy can be safely ignored. However, this is not the case in general. Even from the vantage point of the original Casimir effect, the story remains subtle because the quantum vacuum energy emerges from deformations of the electromagnetic quantum fluctuations, and no simple nonrelativistic limit can be taken; the photon is massless and propagates at the speed of light.

However, in a nonrelativistic setup, one can imagine emergent degrees of freedom, constrained by boundaries, and how these could give rise to nontrivial quantum vacuum phenomena. This has been explored in the context of quantum liquids and Bose-Einstein condensation where (1) contributes to the zero temperature thermodynamic potential (on top of the classical ground state contribution); see, for example, Refs. [18–28].

There are at least two reasons why in a nonrelativistic setting the situation is far from obvious. The first is that any time we are in the presence of interactions and nontrivial boundary conditions, the frequencies ω_n in (1) develop a nontrivial dependence on the ground state of the system. This can be seen using the background field method (see Ref. [12], Sec. 6.7), although computing the frequencies within this framework becomes a hard task. Earlier calculations relying on a perturbative expansion around small coupling exist [29–31], and more recently, Ref. [32] has developed a way to compute the quantum vacuum energy for a relativistic $1+1$-dimensional scalar field theory without relying on expansions in powers of the interaction strength (see also Refs. [33–37]). The second reason has to do with the regularization. In the relativistic case, the quantum vacuum energy emerges from the summation of the entire spectrum as in (1); this summation is divergent and must be regularized. A subtlety with this is due to the existence of a physical cutoff that may alter the spectral sum in (1). Within a lattice approach, this should be possible (see Ref. [14]); however, it is not at all obvious how to do this within an effective field theory approach. It is certainly an interesting question to ask whether any remnant of the quantum vacuum energy remains in the nonrelativistic limit.

For the case of nonlinear models, the difference in the dispersion relation due to the presence of interactions, the presence of external forcing (e.g., rotation), a physical cutoff scale and boundary conditions are all factors that together conjure to induce intricate behaviors in the quantum vacuum energy. Here, we look at the above questions within the paradigmatic nonlinear Schrödinger equation. Our approach to compute the quantum vacuum energy exploits the integrability structure of the nonlinear Schrödinger equation associated with our problem. The calculations are done both using zeta-regularization including the contribution from the whole spectrum, as well as a more physical regularization scheme where the spectral sums are modulated by a frequency dependent window function that suppresses the contribution of the high-energy modes, leaving a dependence on a physical cross-over scale. As we shall see, the two methods lead to compatible results, with the only expected consequence of the cutoff being that of regularizing the vacuum energy at short distance. In conclusion, we will describe how our predictions can, in principle, be measured experimentally with cold-atom rings.

Nonrelativistic Schrödinger model. We shall consider a system of nonrelativistic interacting bosons, described by a complex Schrödinger quantum field $\Phi = (\phi_1 + i\phi_2)/\sqrt{2}$, with $\phi_1, \phi_2 \in \mathbb{R}$, confined to a one-dimensional (1D) ring of radius R, rotating with constant angular velocity Ω. We assume that the periodicity of the ring is externally broken by the presence of a barrier that we describe by imposing Dirichlet boundary conditions at one point on the ring. The Lagrangian density is

$$\mathcal{L} = \frac{i}{2}(\Phi^\dagger\dot{\Phi} - \Phi\dot{\Phi}^\dagger) + \frac{i}{2}\Omega(\Phi^\dagger\Phi' - \Phi\Phi^{\dagger\prime}) - \frac{1}{2mR^2}\Phi^{\dagger\prime}\Phi' - \frac{\lambda}{4}(\Phi^\dagger\Phi)^2, \tag{2}$$

where $0 \le \varphi \le 2\pi$, $x = R\varphi$, $\dot{} = d/dt$, and $' = d/d\varphi$. We set $\hbar = 1$. Expression (2) represents the Lagrangian density of an observer corotating with the ring. In this reference frame, boundary conditions for the corotating observer are time independent [38–40]. The following nonlinear Schrödinger equation can be derived from (2):

$$i\dot{\Phi} = -i\Omega\Phi' - \frac{1}{2mR^2}\Phi'' + \frac{\lambda}{2}|\Phi|^2\Phi. \tag{3}$$

The normal mode decomposition can be carried out by looking for stationary solutions of the form $\Phi(t,\varphi) = e^{-i\omega_p t} f_p(\varphi)$. This allows us to write Eq. (3) as

$$0 = \frac{1}{2mR^2}f_p'' + i\Omega f_p' - \left(\frac{\lambda}{2}|f_p|^2 - \omega_p\right)f_p. \tag{4}$$

To solve (4), we decompose f_p as $f_p(\varphi) = \rho(\varphi)e^{i\alpha(\varphi)}$, with $\rho(\varphi), \alpha(\varphi) \in \mathbb{R}$ that leads to

$$0 = \frac{\rho''}{2mR^2} + \left(\omega_p - \frac{\alpha'^2}{2mR^2} - \Omega\alpha'\right)\rho - \frac{\lambda}{2}\rho^3, \tag{5}$$

$$0 = \frac{\alpha''\rho}{2mR^2} + \frac{1}{mR^2}\alpha'\rho' + \Omega\rho'. \tag{6}$$

The above system of equations can be solved analytically, first obtaining α' in terms of ρ from Eq. (6), $\alpha' = \beta = C/\rho^2 - mR^2\Omega$ (C is an integration constant), and then substituting α' in Eq. (5); this gives rise to a cubic nonlinear equation in ρ that can be solved in terms of Jacobi elliptic functions. Imposition of the boundary conditions selects the solution as a Jacobi `sn` function and leads to the following quantization conditions for the eigenfrequencies. The procedure is straightforward but lengthy. For completeness, we give all the details in the supplemental material [41] and refer the reader to Refs. [42–45] for further details on elliptic equations. The solution can be written as

$$\Phi(t, \varphi) = A_n e^{-i\omega_n t} e^{-i(mR^2\Omega\varphi - \pi/4)} \mathrm{sn}(q_n\varphi, k_n), \tag{7}$$

with the normalization factor A_n expressed in terms of elliptic integrals of the first and second kinds, $K(z)$ and $E(z)$, respectively,

$$A_n^2 = \frac{k_n^2}{2\pi R(1 - E(k_n)/K(k_n))}. \tag{8}$$

The momentum q_n and the elliptic modulus k_n are quantized according to the following relations,

$$q_n = \frac{n}{\pi}K(k_n), \qquad n \in \mathbb{N}, \tag{9}$$

$$\lambda mR\frac{\pi}{4n^2} = K(k_n)(K(k_n) - E(k_n)), \tag{10}$$

where (9) comes from the periodicity of the solution and (10) is derived from the first integral of the equation of motion. Finally, the eigenfrequencies are given by

$$\omega_n = (1 + k_n^2)q_n^2/(2mR^2) - mR^2\Omega^2/2. \tag{11}$$

Details on how to derive Eqs. (7)–(11) are given in the supplemental material [41].

Quantum vacuum energy and spectral asymptotics. A nonrenormalized expression for the quantum vacuum energy (1) can be written as follows (see Ref. [12,46]):

$$\mathscr{E}_r(s) = \frac{\mu^s}{2}\sum_n \omega_n^{1-s}, \tag{12}$$

where $s \in \mathbb{C}$ is a complex-valued regularization parameter and μ is a renormalization scale with dimension of energy. The index r is a reminder that (12) refers to the corotating frame. The eigenvalues ω_n are given in terms of the nonlinear, coupled algebraic equations (9)–(11). The regularization of (12) is done by finding a representation that converges in some region of the complex-s plane, followed by analytical continuation to the physical value $s \to 0$. Here, we use the spectral asymptotics of the eigenvalues and express (12) as

$$\mathscr{E}_r(s) = \Delta + \tilde{\mathscr{E}}_r(s), \tag{13}$$

where

$$\tilde{\mathscr{E}}_r(s) = \frac{\mu^s}{2}\sum_n (\omega_n^{(a)})^{1-s}, \tag{14}$$

and

$$\Delta = \frac{1}{2}\sum_n (\omega_n - \omega_n^{(a)}). \tag{15}$$

The quantity $\omega_n^{(a)}$ represents the asymptotic expansion of the eigenvalues ω_n as a function of the quantum number n. If the asymptotic expansion includes all terms up to $O(1/n^2)$ as we shall do here, then the summand in Δ scales as $O(1/n^2)$, i.e., Eq. (15), and thus converges for $s \to 0$ [in formula (15) we have already set $s \to 0$]. Such a procedure simply confines the divergences to $\tilde{\mathscr{E}}_r(s)$ that will need explicit regularization. The first step of the process is to obtain the asymptotic behavior of the eigenvalues. Since the left-hand side of Eq. (10) converges to zero for $n \to \infty$, while the right-hand side, as a function of k_n, goes to zero only in the limit $k_n \to 0$, while decreasing monotonically for increasing $k_n > 0$, the right-hand side of (10) for small k_n gives the relevant limit to capture the large-n asymptotic behavior $k_n^2 \approx 2\lambda mR/(\pi n^2)$. This result used with (9) and (11) allows us to extract the asymptotic behavior of ω_n:

$$\omega_n^{(a)} = n^2/\eta^2 + \rho^2 + O(1/n^2), \tag{16}$$

where $\eta^2 = 8mR^2$ and $\rho^2 = 3\lambda/(8\pi R) - mR^2\Omega^2/2$. Figure 1 shows a comparison between the eigenvalues computed numerically and their asymptotic counterparts

The large-n scaling of the eigenvalues is consistent with Weyl's law that in the present case predicts a leading large-n behavior of the ω_n scaling as n^2 and independent of λ [47]. Inserting (16) in (14), we get

$$\tilde{\mathscr{E}}_r(s) = \frac{(\mu\eta^2)^s}{2\eta^2}\sum_n (n^2 + \eta^2\rho^2)^{1-s} \tag{17}$$

and the Chowla-Selberg representation [48,49], from which the limit $s \to 0$ can be taken to arrive at the following regularized expression:

$$\tilde{\mathscr{E}}_r = \lim_{s\to 0}\tilde{\mathscr{E}}_r(s) = -\frac{1}{4}\left(\frac{3\lambda}{8\pi R} - \frac{mR^2\Omega^2}{2}\right). \tag{18}$$

The total quantum vacuum energy in the corotating frame is given by $E_r = \tilde{\mathscr{E}}_r + \Delta$. To get the energy in the laboratory

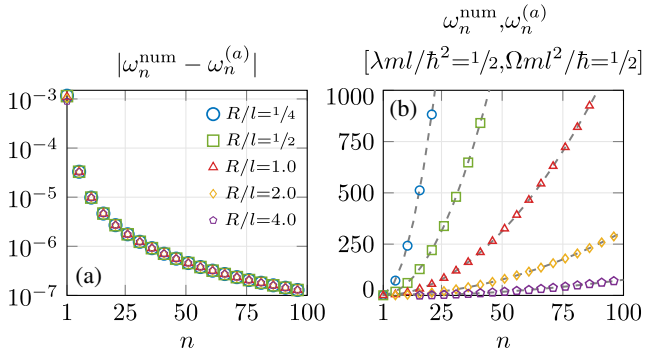

FIG. 1. Comparison between (11) and the eigenvalues computed numerically. Panel (a) shows the absolute difference between the asymptotic and exact nonlinear eigenvalues, while (b) shows individual datasets for fixed R. Colored data in (b) were obtained numerically, while the gray dashed lines were calculated from Eq. (11). Here, $\Omega Rml/\hbar = 0.5$ and $\lambda = ml/\hbar^2 = 0.5$ throughout. Throughout the paper, the quantity l represents a generic unit scale. Corresponding vertical axis labels are displayed above each panel.

frame E_s, one can use $E_s - E_r = \mathbf{\Omega L}$, where $L = -\partial E_r/\partial\Omega$ is the angular momentum [34,38,39,50]:

$$E_s = \Delta - \Omega\frac{\partial\Delta}{\partial\Omega} - \frac{3\lambda}{32\pi R} - \frac{mR^2\Omega^2}{8}. \tag{19}$$

The resulting force $F_s = -\partial E_s/\partial R$ is

$$F_s = -\frac{\partial\Delta}{\partial R} + \Omega\frac{\partial^2\Delta}{\partial\Omega\partial R} - \frac{3\lambda}{32\pi R^2} + \frac{mR\Omega^2}{4}. \tag{20}$$

Ignoring the contributions from Δ, the above expression comprises a contribution proportional to $-\lambda/R$ that vanishes for $\lambda \to 0$ and scales as the inverse of the ring size: this is an attractive "Casimir-like" contribution. The other contribution $E_{\mathcal{I}} = \frac{1}{2}\mathcal{I}_{\mathcal{R}}\Omega^2$ is proportional to the moment of inertia of the ring $\mathcal{I}_R = mR^2$ with radius R. The vanishing behavior for $\lambda \to 0$ and $\Omega \to 0$ is consistent with the fact that the quantum vacuum energy should vanish in the absence of interactions and rotation. The angular velocity appears as the square of Ω, and this is again consistent with the fact that our model does not include parity breaking terms; thus, the energy should be symmetric with respect to $\Omega \leftrightarrow -\Omega$. The force vanishes at the critical radius

$$R_{\rm crit} \approx \sqrt[3]{\frac{3\lambda}{8\pi m\Omega^2}}, \tag{21}$$

with its sign changing from negative-attractive for $R < R_{\rm crit}$ to positive-repulsive for $R > R_{\rm crit}$. Interestingly, also the way the force scales with the ring size changes with the angular velocity: it scales linearly in the regime of fast rotation, while it scales as the inverse square of the ring size for slow rotation. The symbol "≈" in (21) indicates that the contribution of Δ has been ignored. Units of $\hbar$ are restored in the numerics, and in what follows, l denotes a generic length scale. Figure 2 shows the quantum vacuum energy (panels a and c) as a function of radius R and rotation strength Ω, respectively, while the two lower panels (b and d) show the corresponding force associated with each dataset from (a) and (c). The gray shaded region shows the parameter regime where the force is repulsive. Figure 3 shows heat maps of Eq. (21) in the (R, Ω) and (R, λ) parameter spaces, (a) and (b), respectively. In panel (a), the interaction strength is $\lambda ml/\hbar^2 = 10$, while the rotation strength is $\Omega ml^2/\hbar = 5$ in (b). The solid blue lines in both panels show the border between the repulsive regime and the causality limit defined by $\Omega Rml/\hbar = 1$. The red dashed line indicates where the force changes sign, obtained from Eq. (21). The red data point in each panel corresponds to the point $(R_\circ, \Omega_\circ)$ in (a) and $(R_\circ, \lambda_\circ)$ in (b) where Eq. (21) and the causality limit coincide, and

$$(R_\circ, \Omega_\circ) = \left(\frac{3}{8\pi}\frac{\lambda ml^2}{\hbar^2}, \frac{8\pi}{3}\frac{\hbar^2}{m^2l^3}\frac{1}{\lambda}\right). \tag{22}$$

The point defined by Eq. (22) in Fig. 3 shows the maximum rotation strength where repulsive solutions are obtained; then, the model of Eq. (3) is expected to support a causal repulsive force in the region $\Omega_c < \Omega < R^{-1}(ml/\hbar)$ and

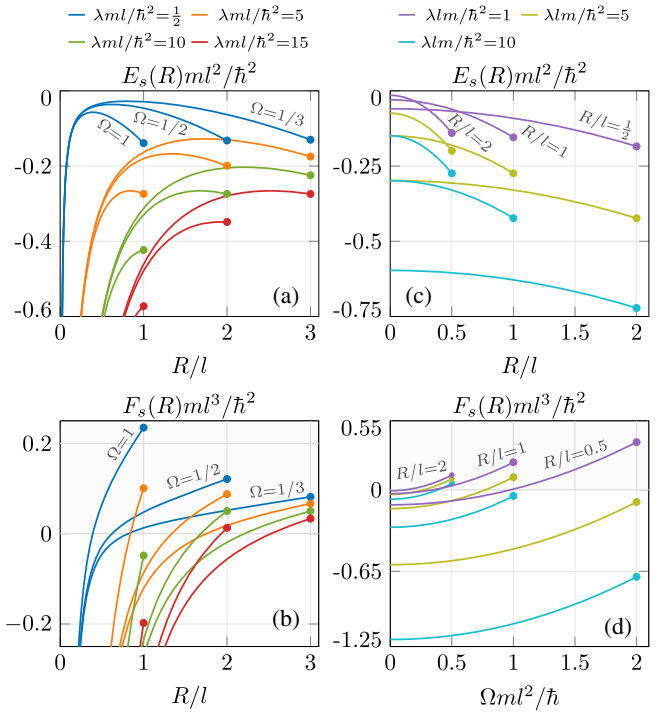

FIG. 2. Quantum vacuum energy and force. Panels (a) and (c) show the quantum vacuum energy, Eq. (19), for the same λ (color groups) and varying Ω (panel (a) or R (panel (c) (see text labels). Panels (b) and (d) show the corresponding force, Eq. (20), for each dataset. The light gray shading indicates the parameter regions where the force changes sign from attractive to repulsive. Corresponding vertical axis labels are displayed above each panel.

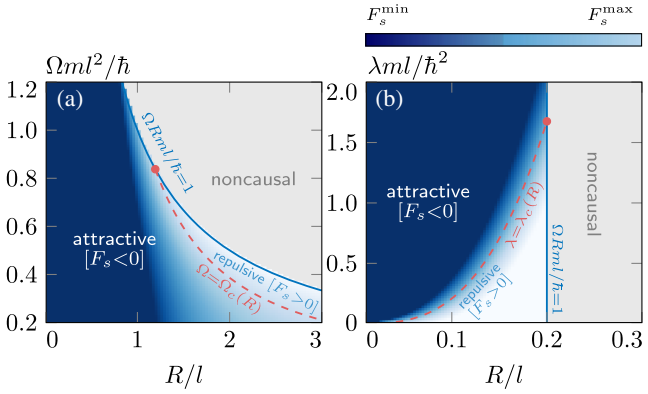

FIG. 3. Quantum fluctuation induced-force heat maps. Panel (a) shows Eq. (20) in the limit $\Delta = 0$ in the (Ω, R) parameter space for fixed $\lambda ml/\hbar^2 = 10$. The solid blue line indicates the border between the repulsive and noncausal regions, while the dashed red line indicates the point at which the force changes sign. Panel (b) shows the magnitude of the force in the (λ, R) parameter space for fixed $\Omega ml^2/\hbar = 5$.

$R > R_\circ$. Likewise for panel (b), the causal repulsive regime is defined between $0 < \lambda < \lambda_c$ and $0 < R < R_\circ$. An analysis, qualitatively similar to Fig. 3(b), can be done for the (R, Ω) parameter space with constant λ.

A subtle point has to do with how the above results will change in the presence of a cutoff scale associated with a minimal length scale (e.g., the interatomic separation scale). We address this question by modifying the regularization procedure to include a frequency-dependent *window function*. This is implemented by defining

$$\tilde{\mathscr{E}}_r = \frac{1}{2}\sum_n \omega_n^{(a)} \sigma_n(\ell_c) \tag{23}$$

and the residual Δ as

$$\Delta = \frac{1}{2}\sum_n (\omega_n - \omega_n^{(a)})\sigma_n(\ell_c). \tag{24}$$

Here, we choose the window function as follows,

$$\sigma_n(\ell_c) = \exp(-\ell_c n^2/(8mR^2)), \tag{25}$$

with the argument of the exponential set by the leading large-n asymptotics of the spectrum. The cutoff scale ℓ_c determines how high-frequency modes are suppressed. The limit $\ell_c \to 0$ of (23)–(24) returns the nonregularized expression for $\tilde{\mathscr{E}}_r$ discussed earlier. While the choice of $\sigma_n(\ell_c)$ is arbitrary, Eq. (25) allows us to write (23) as

$$\tilde{\mathscr{E}}_r = -\frac{\rho^2}{4} + \frac{\rho^2}{4}\theta_3\left(\frac{\ell_c}{\pi\eta^2}\right) - \frac{1}{4\pi\eta^2}\theta_3'\left(\frac{\ell_c}{\pi\eta^2}\right), \tag{26}$$

where θ_3 is the following Jacobi *thetanull* function [51], $\theta_3(x) = \sum_{n=-\infty}^{\infty} e^{-\pi x n^2}$. This choice of regularization has the advantage that the first term of (26) corresponds to the fully resummed result and the effect of the cutoff is encoded in the latter two terms of (26). Proving the consistency of the two approaches, with and without the cutoff, requires care since in the limit $\ell_c \to 0$ the theta function diverges and requires regularization. The theta function can be regularized by requiring that the cutoff-dependent contribution in (26) vanishes in the limit of $\ell_c \to 0$, corresponding to a subtraction of the divergent contribution. To compute the finite $\ell_c \to 0$ limit of (26), we use the modular transformation $\theta_3(x) = \sqrt{1/x}\theta_3(1/x)$ along with the small-x expansion of the theta function [51], leading to $\theta_3(x) \approx 1/\sqrt{x} + O(\exp(-\pi/x)/\sqrt{x})$. Using this expression in (26) and removing the divergent part, consistently with the regularization of the theta function, gives the expected fully resummed result. The corrections due to the cutoff near $R \sim R_{\rm crit}$ to the fully resummed result can be estimated assuming that $\ell_c \ll R_{\rm crit}$ and can be computed including higher order corrections in the expansion of the theta function,

$$\theta_3(x) - 1/\sqrt{x} \approx 2\sigma/\sqrt{x} + 2\sigma^4/\sqrt{x} + O(\sigma^9/\sqrt{x}), \tag{27}$$

where $\sigma = \exp(-\pi/x)$. Using (27) in (26) implies that corrections to the fully resummed result are exponentially small; that is, the behavior of the vacuum energy is robust against the inclusion of a cutoff smaller than the critical radius for large enough ring size. For small R, we expect the cutoff to regulate the diverging $1/R$ behavior of the leading term in Eq. (26). Expanding the theta functions in (26) for ℓ_c/R^2 large gives at leading order

$$\tilde{\mathscr{E}}_r \approx \frac{\rho^2 - \eta^{-2}}{2} e^{-\ell_c/\eta^2} \underset{R\to 0}{\longrightarrow} 0, \tag{28}$$

which can be contrasted with the $\rho^2 \sim R^{-2}$ behavior of the vacuum energy as obtained by full resummation.

Conclusions. The behavior of the quantum vacuum energy of an interacting nonrelativistic system is far from trivial. Here, we have looked at an example of this using a nonlinear Schrödinger quantum field theory and computed the quantum vacuum energy and force without resorting to any perturbative expansion in the coupling constant, simply relying on the exact integrability of the nonlinear problem. The novel results are summarized in the "phase diagram" of Fig. 3, which shows how the fluctuation-induced force as a function of rotation and interaction strength separates into a noncausal region plus an attractive-repulsive region. This behavior arises from the stabilization between an attractive Casimir-like component and a repulsive centrifugal one.

An interesting potential connection seems evident between our quantum field theoretical setup and the area of ultracold atoms. A possibly relevant example is the setup of Ref. [52], which consists of a ^{23}Na Bose-Einstein condensate confined in a ring of size $R \sim 20$ μm. Within a quasi-1D approximation, the interaction strength λ can be expressed in terms of the scattering length a_s, and the transverse length scale l can be expressed as $\lambda = g/(\pi l^2)$

(here, $g = 4\pi\hbar^2 a_s/m$ defines the atomic interaction with $a_s = 50a_0$ for ^{23}Na) [53]. Taking $l \sim 2$ μm to ensure that $l \ll R$ and assuming a condensate of $N = 2 \times 10^3$ atoms allows us to arrive at a dimensionless interaction strength $\lambda m l/\hbar^2 \sim 4a_s N/l$, which, using the above parameter values, gives $4a_s N/l \sim 10$, a value close to that used in Fig. 3(a). The force F_s can also be estimated in a similar manner; using Eq. (20) and the above definitions, we obtain a dimensionless force:

$$F_s \frac{ml^3}{\hbar^2} = -\frac{3}{8\pi}\frac{a_s N l}{R^2} + \frac{m^2 l^3}{\hbar^2}\frac{R\Omega^2}{4}. \tag{29}$$

Using a rotation speed of $\Omega \sim 2\pi \times 25$ Hz from the experiment of Ref. [54], we obtain $F_s ml^3/\hbar^2 \sim 0.1$, modest but potentially large enough to be observable in a future experiment. Using these values, a ring of size $R \sim 20$ μm would fall in the causal repulsive region of Fig. 3(a), and $\Omega ml^2/\hbar \sim 0.2$ favoring lower rotation frequencies. In this work, Dirichlet boundary conditions have been used, which could be simulated using a weak link as realized in the Bose-Einstein condensation ring experiments of Refs. [55,56].

The physical system described in this work has potential applications in atomtronics [57], facilitating an additional opportunity to explore the fundamental physics associated with the quantum vacuum. Extensions to systems of fermions [58] or with multiply connected geometries [59] offers additional avenues to explore the effects described in this work in uncharted scenarios.

Acknowledgments. The research of A. F. was supported by the Japanese Society for the Promotion of Science Grant-in-Aid for Scientific Research (KAKENHI, Grant No. 21K03540). The research of M. E. was supported by the Australian Research Council Centre of Excellence in Future Low-Energy Electronics Technologies (Project No. CE170100039), funded by the Australian Government, and by the Japan Society of Promotion of Science Grant-in-Aid for Scientific Research (KAKENHI Grant No. JP20K14376). A. F. and M. E. acknowledge support from the University of Queensland (SMP Accelerator Grant). We would like to thank G. Marmorini for discussions.

[1] Y. Takahashi and H. Shimodaira, Nuovo Cimento Soc. Ital. Fis. **62A**, 255 (1969).
[2] G. Plunien, B. Muller, and W. Greiner, Phys. Rep. **134**, 87 (1986).
[3] L. H. Ford, Phys. Rev. D **11**, 3370 (1975).
[4] H. B. G. Casimir, Proc. K. Ned. Akad. Wet. **51**, 793 (1948).
[5] K. A. Milton, *The Casimir Effect* (World Scientific, Singapore, 2001).
[6] M. Bordag *et al.*, *Advances in the Casimir Effect* (Oxford University Press, New York, 2009).
[7] S. K. Lamoreaux, Phys. Rev. Lett. **78**, 5 (1997).
[8] U. Mohideen and A. Roy, Phys. Rev. Lett. **81**, 4549 (1998).
[9] G. Bressi, G. Carugno, R. Onofrio, and G. Ruoso, Phys. Rev. Lett. **88**, 041804 (2002).
[10] T. Gong *et al.*, Nanophotonics **10**, 523 (2020).
[11] G. C. Matos, R. de Melo e Souza, P. A. Maia Neto, and F. Impens, Phys. Rev. Lett. **127**, 270401 (2021).
[12] D. J. Toms, *The Schwinger Action Principle and Effective Action* (Cambridge University Press, Cambridge, England, 2012).
[13] D. J. Toms, Phys. Rev. A **66**, 013619 (2002).
[14] K. Nakayama and K. Suzuki, Phys. Rev. Res. **5**, L022054 (2023).
[15] M. V. Cougo-Pinto, C. Farina, J. F. M. Mendes, and A. C. Tort, Braz. J. Phys. **31**, 45 (2001).
[16] E. B. Kolomeisky, H. Zaidi, L. Langsjoen, and J. P. Straley, Phys. Rev. A **87**, 042519 (2013).
[17] O. Corradini, A. Flachi, G. Marmorini, M. Muratori, and V. Vitagliano, J. Phys. A **54**, 405401 (2021).
[18] A. Recati, J. N. Fuchs, C. S. Peça, and W. Zwerger, Phys. Rev. A **72**, 023616 (2005).
[19] D. C. Roberts and Y. Pomeau, Phys. Rev. Lett. **95**, 145303 (2005).
[20] A. Edery, J. Stat. Mech. (2006) P06007.
[21] J. Schiefele and C. Henkel, J. Phys. A **42**, 045401 (2009).
[22] S. Biswas, J. K. Bhattacharjee, D. Majumder, K. Saha, and N. Chakravarty, J. Phys. B **43**, 085305 (2010).
[23] M. Schecter and A. Kamenev, Phys. Rev. Lett. **112**, 155301 (2014).
[24] A. Diallo and C. Henkel, J. Phys. B **48**, 165302 (2015).
[25] N. Van Thu and L. Thi Theu, J. Stat. Phys. **168**, 1 (2017).
[26] J. Marino, A. Recati, and I. Carusotto, Phys. Rev. Lett. **118**, 045301 (2017).
[27] P. Song and N. Van Thu, J. Low Temp. Phys. **202**, 160 (2021).
[28] P. T. Song, Phys. Lett. A **455**, 128515 (2022).
[29] L. H. Ford, Proc. R. Soc. A **368**, 305 (1979).
[30] D. J. Toms, Phys. Rev. D **21**, 928 (1980).
[31] C. Peterson, T. H. Hansson, and K. Johnson, Phys. Rev. D **26**, 415 (1982).
[32] M. Bordag, Universe **7(3)**, 55 (2021).
[33] H. W. Blöte, J. L. Cardy, and M. P. Nightingale, Phys. Rev. Lett. **56**, 742 (1986).
[34] A. Flachi and M. Edmonds, Phys. Rev. D **107**, 025008 (2023).
[35] A. Flachi, Phys. Rev. Lett. **110**, 060401 (2013).
[36] A. Flachi, M. Nitta, S. Takada, and R. Yoshii, Phys. Rev. Lett. **119**, 031601 (2017).
[37] A. Flachi and V. Vitagliano, J. Phys. A **54**, 265401 (2021).
[38] M. N. Chernodub, Phys. Rev. D **87**, 025021 (2013).

[39] M. Schaden, arXiv:1211.2740.
[40] E. Ambrus and E. Winstanley, Phys. Lett. B **734**, 296 (2014).
[41] See Supplemental Material at http://link.aps.org/supplemental/10.1103/PhysRevD.108.L121702 for the details of the solutions of the equations of motion.
[42] M. Lakshmanan and S. Rajasekar, *Nonlinear Dynamics: Integrability, Chaos and Patterns* (Springer, Berlin, 2003).
[43] L. D. Carr, C. W. Clark, and W. P. Reinhardt, Phys. Rev. A **62**, 063610 (2000).
[44] L. D. Carr, C. W. Clark, and W. P. Reinhardt, Phys. Rev. A **62**, 063611 (2000).
[45] A. Sacchetti, J. Phys. A **53**, 385204 (2020).
[46] E. Elizalde *et al.*, *Zeta-Regularization Techniques with Applications* (World Scientific, Singapore, 1994).
[47] H. P. Baltes and E. R. Hilf, *Spectra of Finite Systems* (Bibliographisches Institute, Zurich, 1976).
[48] See formula (43) of A. Flachi and T. Tanaka, Phys. Rev. D **78**, 064011 (2008).
[49] E. Elizalde, Commun. Math. Phys. **198**, 83 (1998).
[50] L. D. Landau and E. M. Lifshitz, *Fisica Statistica* (Editori Riuniti, Roma, 1978).
[51] B. C. Berndt, *Ramanujan's Notebooks, Part III* (Springer, Berlin, 1991); *Ramanujan's Notebooks, Part V* (Springer, Berlin, 1998).
[52] S. Eckel, J. G. Lee, F. Jendrzejewski, N. Murray, C. W. Clark, C. J. Lobb, W. D. Phillips, M. Edwards, and G. K. Campbell, Nature (London) **506**, 200 (2014).
[53] C. Samuelis, E. Tiesinga, T. Laue, M. Elbs, H. Knöckel, and E. Tiemann, Phys. Rev. A **63**, 012710 (2000).
[54] S. Pandey, H. Mas, G. Drougakis, P. Thekkeppatt, V. Bolpasi, G. Vasilakis, K. Poulios, and W. von Klitzing, Nature (London) **570**, 205 (2019).
[55] C. Ryu, P. W. Blackburn, A. A. Blinova, and M. G. Boshier, Phys. Rev. Lett. **111**, 205301 (2013).
[56] F. Jendrzejewski, S. Eckel, N. Murray, C. Lanier, M. Edwards, C. J. Lobb, and G. K. Campbell, Phys. Rev. Lett. **113**, 045305 (2014).
[57] L. Amico *et al.*, AVS Quantum Sci. **3**, 039201 (2021).
[58] Y. Cai, D. G. Allman, P. Sabharwal, and K. C. Wright, Phys. Rev. Lett. **128**, 150401 (2022).
[59] T. Bland, I. V. Yatsuta, M. Edwards, Y. O. Nikolaieva, A. O. Oliinyk, A. I. Yakimenko, and N. P. Proukakis, Phys. Rev. Res. **4**, 043171 (2022).